A&A 386, 899–909 (2002)
DOI: 10.1051/0004-6361:20020282

Astronomy & Astrophysics

Low resolution spectroscopy of ISOGAL sources: Search for early-type stars with infrared excess⋆,⋆⋆,⋆⋆⋆

M. Schultheis[1], M. Parthasarathy[2,3], A. Omont[1], M. Cohen[4], S. Ganesh[5], F. Sevre[1], and G. Simon[6]

[1] Institut d'Astrophysique de Paris, CNRS, 98bis Bld. Arago, 75014 Paris, France
[2] Indian Institute of Astrophysics, Koramangala, Bangalore 560034, India
[3] National Astronomical Observatory of Japan, 2-21-1 Osawa, Mitaka, Tokyo 181-8588, Japan
[4] Radio Astronomy Laboratory, University of California, Berkeley, CA 94720, USA
[5] Physical Research Laboratory, Navarangpura, Ahmedabad 380009, India
[6] DASGAL CNRS UMR 8633, Observatoire de Paris, France

Received 8 August 2001 / Accepted 22 February 2002

Abstract. An analysis of low resolution spectra and infrared data of 29 ISOGAL-DENIS sources with mid-IR excess is presented. Eight ISOGAL sources from our sample with 7–15 μm excesses are found to be B and A-type stars, some of them with emission lines. Two ISOGAL sources, J175614.4-240831 (B3-4IIIe) and J173845.3-312403 (B7IIIe), show a bump between 5000 and 6000 Å which may be attributed to extended red emission (ERE). Some of the B, A and F-type giants with a large infrared excess might be in the post-AGB phase.
For about 50% of the sources in this preliminary study, a nearby second (or even multiple) component was found. Such sources, in particular two B-stars, are not discussed when the probability of the optical spectrum being associated with the ISOGAL source is low. These results confirm that the DENIS-ISOGAL $I-J/K$–[15] diagram is the most suitable diagram to distinguish between early (AB) and late spectral types (KM). It provides the most useful tool to systematically search for nearby early-type stars with an infrared excess among the background of distant AGB stars in ISOGAL fields of the Galactic disk.

Key words. stars: AGB and post-AGB – stars: early-type – Galaxy: solar neighbourhood – ISM: reflection nebulae – ISM: dust, extinction

1. Introduction

Infrared dust emission is one of the best tools for tracing circumstellar matter in various phases of stellar evolution: cocoons and disks in star formation, mass-loss (and circumstellar disks) in various classes of evolved stars, Vega-type disks, etc.

Surveys with the ISO satellite, especially with the ISOCAM instrument (Cesarsky et al. 1996), have opened new possibilities with a sensitivity typically two orders of magnitude better than IRAS and an angular resolution ten times better. The ISOGAL 7 and 15 μm survey (Omont et al. 2002) has observed $\sim$16 deg^2 distributed in the most obscured regions of the central Galaxy. The total number of stars detected ($\sim 10^5$) is comparable to the number of stars detected by IRAS in the entire Galaxy. ISOGAL and DENIS (or 2MASS) near-infrared data constitute a powerful combination for identifying the nature of ISOGAL sources even in regions of high extinction (A_v up to 20–30). The various colour-colour and colour-magnitude diagrams from the photometry in the five ISOGAL-DENIS bands provide a wealth of information on the extinction, distance, intrinsic colours and absolute magnitudes. Most sources are M giants at several kpc, with a few foreground K-giants, as observed by Ojha et al. (2000). Among these M-type sources, a large proportion of those detected at 15 μm are AGB-LPVs with a variety of mass-loss rates which are well assessed by the 15 μm excesses (Omont et al. 1999; Glass et al. 1999; Alard et al. 2001).

It is expected that this large sample of infrared sources contains a number of non-AGB stars with circumstellar material like Herbig Ae/Be stars, various types of post-AGB stars, and other peculiar objects. Although the various colours and magnitudes offer broad diagnostics, spectroscopic information is desirable to better characterise them and to identify their exact nature. We have thus begun a systematic spectroscopic study of peculiar ISOGAL sources, with the main goal to identify accretion and

Send offprint requests to: M. Schultheis,
e-mail: schulthe@iap.fr

⋆ This is paper No. 9 in a refereed journal based on data from the ISOGAL project.

⋆⋆ Based on observations with ISO, an ESA project with instruments funded by ESA Member States (especially the PI countries: France, Germany, The Netherlands and the UK) and with the participation of ISAS and NASA.

⋆⋆⋆ Based on observations collected at the European Southern Observatory, La Silla Chile (63.L-0319).

post-accretion disks, post-AGB stars and Vega-type stars. Selection criteria are designed to select hotter nearby stars with mid-IR excess while avoiding AGB stars. We report here the results of a preliminary study of low-resolution spectroscopy of a sample of 29 candidate objects.

2. Observations

Medium resolution spectra of 29 ISOGAL sources were obtained with the Danish 1.54 m telescope at ESO, La Silla (Chile), equipped with the DFOSC instrument. The observations were carried out between 23–30 June 1999. 60% of the time was lost due to bad weather.

The spectra were recorded on a Loral/Lesser 2052 × 2052 pixel CCD chip, and cover a wavelength range from 3500 Å to 8200 Å with a resolution of 3 Å/pixel. The objects were observed through a 2″ slit. Before each spectrum an R-band image was taken. During the night a 10 s exposure with a Ne-Ar lamp was made for calibration of the wavelength scale. At the beginning and at the end of each night one flux standard was observed (Feige 110 and Wolf 485a) through a 5″ slit. The observations were performed under photometric conditions.

2.1. The sample

Due to the limiting sensitivity of the instrument, only sources with $I \lesssim 14$ were chosen. Such a condition excludes more than 90% of ISOGAL sources, since they suffer high extinction, as well as most AGB stars in the inner disk/bulge and most young stars with circumstellar and interstellar reddening. Therefore, with very few exceptions, the selected sources are expected to be foreground, relatively nearby ($\lesssim$1–2 kpc), objects. We have chosen mainly sources with large values of $K_{\rm S}-[15]$ and $[7]-[15]$ with respect to $J-K$ and $I-J$. This implies the presence of circumstellar dust in a shell or disk.

Our objects were selected from a prelimary version of the ISOGAL catalog but in the analysis reported here, we use the final ISOGAL catalog (Omont et al. 2002; Schuller et al. 2002). The DENIS observations form part of a dedicated survey of the Galactic Bulge (Simon et al., in preparation). The 2MASS data, when available, were taken from the second incremental data release (Skrutskie 1998).

Table 1 summarises the ISOGAL sources observed, including their DENIS, 2MASS and ISOGAL magnitudes as well as the projected distance in arcsecond between the apparently associated DENIS and ISOGAL sources.

3. Data reduction

All reduction procedures were carried out with the MIDAS software package. After removal of cosmic ray events, subtraction of the bias level and the dark current, all CCD frames were divided by a normalized flat field. Two sky frames were taken, left and right of the object and the mean sky was subtracted from the object. For the wavelength calibration, 12 Ne-Ar lines were used which led to a rms error for each spectrum of about 0.2 Å. The spectra were rebinned to a linear scale, with a resolution of 3 Å/pixel. The two photometric standards Wolf 485a and Feige 110 (Stone 1977; Massey & Strobel 1988) were used for flux calibration. All spectra were calibrated with the averaged instrumental response from the two standards and were corrected for atmospheric extinction. Typical errors in the absolute fluxes are ∼10%.

4. Analysis

4.1. Spectral classification

Figure 1 shows a sample of the resulting spectra (F_λ in erg s^{-1} cm^{-2} Å^{-1}), normalized to unity by the flux at 5500 Å. The most prominent spectral features are indicated. A wide variety of spectral types is present. We classified the optical spectra of our sources by comparing them with the spectra of standard stars drawn from the low-resolution spectral atlases of Jacoby et al. (1984), Torres-Dodgen & Weaver (1993), Pickles (1998), Walborn (1980) and Yamashita et al. (1977). The spectral types are given in Table 1. Some of our program stars show significant reddening and, therefore, the blue part of the spectrum shortward of 5000 Å does not have a high signal-to-noise ratio. When the reddening is high, we have used the red part of the spectrum of our program stars for classification. The spectral atlases of Turnshek et al. (1985), Walborn (1980) and Torres-Dodgen & Weaver (1993) were useful in the red spectral region for both hot and cool stars. The uncertainty in our assigned spectral types is estimated to be two subtypes, while (due to the low resolution of our spectra) the uncertainty in the luminosity should be one subclass.

4.2. Interstellar reddening

We derived a rough effective temperature for each object using the corresponding Kurucz models. The total (interstellar + circumstellar) reddening has been obtained adopting the value which gave the best fit between the observed spectrum and the reddened model spectrum (Fig. 4). This method depends strongly on the adopted fundamental parameters ($T_{\rm eff}$, log g, log Z) of the Kurucz models and on the slope of the observed spectrum.

Thus we estimate the uncertainty of $E(B-V)$ for spectral types $B-F$ of the order of ∼0.3 while, for later spectral types (KM), we have larger errors (∼0.5) as the Kurucz models do not reproduce cool stellar spectra well. The corresponding $E(B-V)$ values are given in Table 1.

4.3. Rejection of dubious cases

Our aim was to characterize the objects and to search for clear cases of mid-infrared excess in stars with spectral types no later than K. We will thus focus the subsequent analysis on such cases, while we report non-confirmed, the most ambiguous cases, and M-stars in Appendix A, and

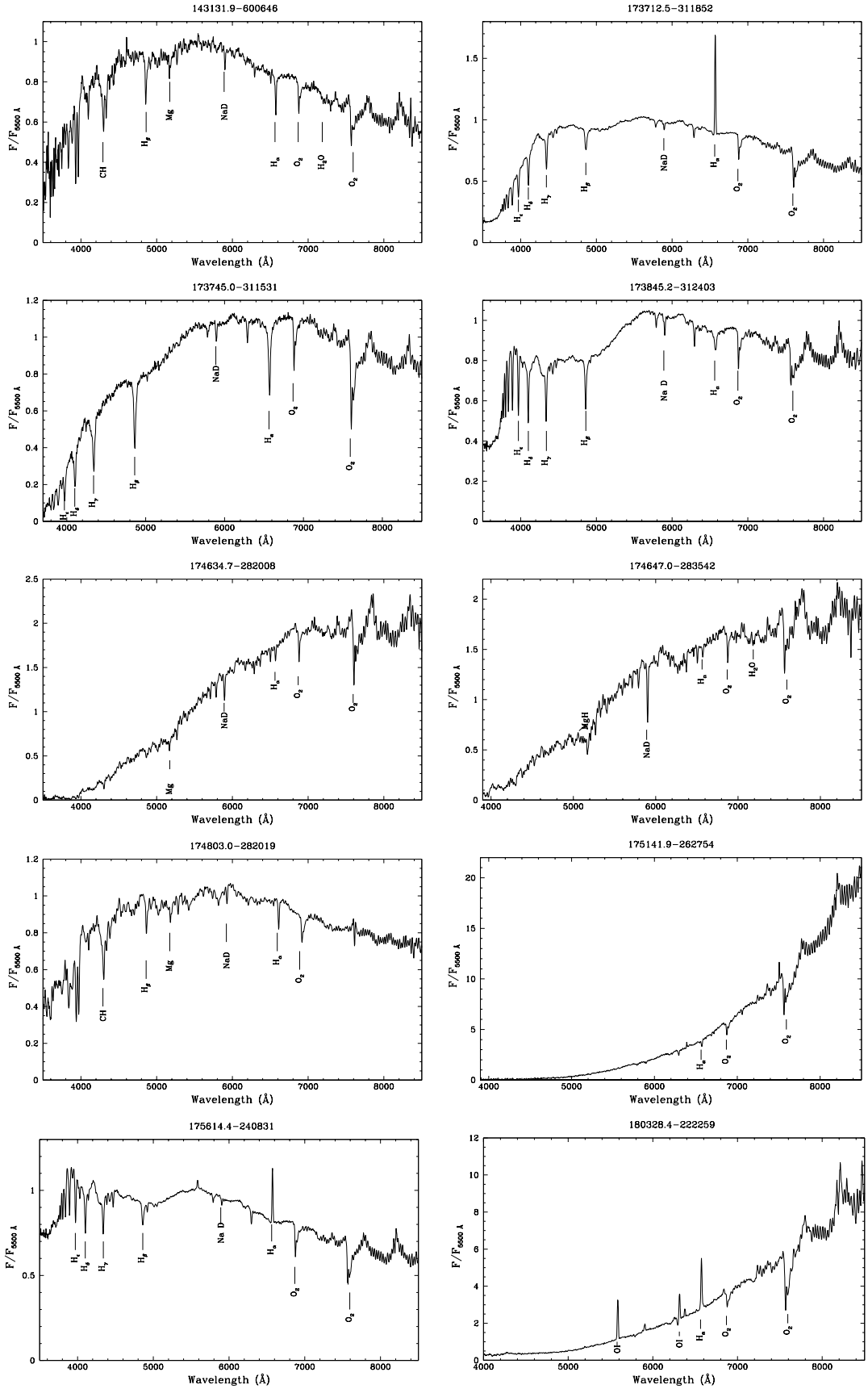

Fig. 1. Sample of optical spectra of ISOGAL sources which are discussed in the main text with the main line identifications. The spectra are normalized to unity at 5500 Å.

Table 1. Coordinates (J2000), magnitudes (DENIS, ISOGAL and 2MASS) of the observed sources as well as the projected distance (in arcsec) between the ISOGAL source and the DENIS counterpart, spectral type, $E(B-V)$ derived by comparison with the Kurucz models. The last column specifies whether the object is discussed in the main text (M) or has been rejected and therefore listed in the Appendix A.

#	ISOGAL PJ	I	J	K_S	[7]	[15]	J_{2MASS}	H_{2MASS}	K_{2MASS}	dist.	Sp.type	$E(B-V)$	Flag
1	143131.9-600646	14.0	8.7	5.8*	5.6	4.3	–	–	–	0.5	F8-G0III	0.2	M
2	143313.2-603705	11.5	10.0	9.0	5.2	4.5	–	–	–	0.9	K4III-II	0.2	A
3	164825.8-441403	14.5	11.6	9.7	9.1	6.6	–	–	–	1.4	K4III-II	1.2	A
4	165019.1-435927	14.7	12.3	9.6	7.2	6.6	–	–	–	1.7	K3III-V	1.0	A
5	165102.4-443738	13.5	12.9	10.0	7.9	7.3	–	–	–	3.2	G4III	0.1	A
6	172001.7-371024	11.4	10.7	10.2	9.6	7.9	–	–	–	0.4	G4III	0.1	A
7	172807.6-331812	13.5	11.3	10.1	8.9	8.6	11.3	10.4	10.2	2.2	G8III-V	1.0	A
8	172830.3-332214	10.7	9.5	8.5	7.8	7.7	9.5	8.7	9.2	2.0	K2III-II	0.1	A
9	172823.5-351559	13.7	8.3	6.0	5.6	4.4	8.4	6.7	5.9	1.5	M5III	2.6	A
10	173219.0-334751	15.1	12.0	8.9	5.1	3.1	11.7	10.1	8.7	1.7	Be-Ae	2.5	A
11	173221.5-335405	13.4	9.3	6.9	6.5	6.3	9.2	7.5	6.9	0.2	M5III	2.0	A
12	173223.0-320841	12.2	9.8	8.3	7.7	7.2	9.8	8.6	8.2	1.1	K5III-II	0.7	A
13	173537.4-335753	14.3	11.9	9.8	7.3	4.8	11.8	10.5	9.7	0.6	lateF	1.5	A
14	173712.5-311852	11.0	10.2	9.7	8.7	7.8	10.2	9.8	9.7	0.7	B8IIIe	0.3	M
15	173745.0-311531	13.4	12.3	11.3	9.8	7.9	12.2	11.8	11.4	0.5	A0III	0.6	M
16	173845.2-312403	11.0	9.8	9.4	9.0	–	9.9	9.6	9.5	1.9	B7IIIe	0.5	M
17	174634.7-282008	11.6	9.8	8.7	7.8	6.3	9.8	8.9	8.7	2.5	K4III	0.3	M
18	174647.0-283542	12.1	10.5	9.3	8.0	7.1	10.5	9.7	9.3	1.5	K5III-II	0.2	M
19	174650.3-284451	13.1	12.1	10.9	8.5	–	12.2	11.7	10.9	1.4	B9III	0.7	A
20	174717.0-290144	11.1	8.6	7.0	6.4	6.2	8.6	7.4	6.9	2.1	lateG	1.7	A
21	174735.9-274633	13.4	10.7	9.6	8.3	7.3	–	–	–	1.7	M6III	0.2	A
22	174803.0-282019	12.6	11.9	11.3	8.0	7.1	11.9	11.5	11.1	1.6	G2III	0.1	M
23	174804.2-281028	13.2	10.6	9.0	9.2	–	10.6	9.5	8.9	0.4	K4III-II	1.5	A
24	174812.1-282319	11.0	8.4	6.7	6.4	6.3	8.3	7.1	6.6	0.9	M2III	0.2	A
25	174819.8-280513	14.1	12.1	10.0	7.7	7.5	–	–	–	0.9	K4III	1.0	A
26	175141.9-262754	12.8	10.0	8.8	7.7	4.0	10.1	9.3	8.8	1.5	early-type	3.2	M
27	175614.4-240831	11.2	10.4	9.9	9.0	8.3	10.3	10.1	9.8	1.0	B3-4IIIe	0.5	M
28	180328.4-222259	13.0	10.5	9.1	7.0	7.3	–	–	–	1.0	early-type	2.5	M
29	180446.3-300318	12.2	9.1	7.6	6.6	5.5	–	–	–	1.2	M7III	0.2	A

* Saturated in DENIS.

in figures available electronically at CDS. Such rejected sources are relatively numerous (∼50%) because of the preliminary nature of our selection criteria and of the quality of data available at the time of the observations. The major cause of rejection (see Appendix A) is evidence of multiple sources in the field with a large probability of false association of a foreground visible star with a distant AGB star, invisible at optical wavelengths. For each individual source, the DENIS/2MASS images in *I, J, H* and K_S and the ISOCAM images in 7 and 15 μm were examined by eye in order to check the cross-identification of the ISOGAL source with the near-IR counterpart. For about 50% of the sources, a second object was found close by, or even multiple components (see the description of the individual objects). When the projected distance to the second source is less than 3.5″ (the search radius for ISOGAL-DENIS associations) we have carefully considered the possible association of the ISOGAL source with the second DENIS source (though we took the optical spectrum of the primary candidate). In addition, we used the $(I-J)_0/(J-K)_0$ diagram (see Fig. 3b) to decide if those objects follow the expected temperature sequence in the colour-colour diagram indicated by the straight lines in Fig. 3b.

The objects with a second nearby source (<3.5″) for which the position in the colour-colour diagram (see Fig. 3b) does not agree with the temperature sequence, were rejected from further discussion (see Appendix).

In addition, we have also rejected the five identified M-stars, and star #23 where the present higher quality ISOGAL fluxes do not confirm the existence of a mid-infrared excess.

4.4. Notes on individual objects

#1: In the colour-magnitude diagrams (see Figs. 2 and 3), this (F8-G0III) star, with narrow Balmer lines, shows a very strong near-IR excess and a moderate mid-IR excess. The SED of this object (see Fig. 4) shows evidence for the presence of hot circumstellar dust with a temperature ∼1500 K. Because our spectra are obtained with a slit spectrograph and the amount of light going through the slit depends on the slit width and "seeing", it is hard to estimate the exact optical flux in units of ergs/cm^2/s.

However, we find that the ratio of integrated IR flux to integrated optical is about 50 which indicates that the central star of object #1 is significantly obscured. This high flux ratio between the IR and optical flux is similar to that of post-AGB stars with dusty disks such as the Red Rectangle or Hen 401 (Parthasarathy et al. 2001). We find a small reddening of $E(B-V) \sim 0.2$ indicating that we see only the scattered starlight in the Optical. High-resolution imaging in the IR may reveal the dusty disk and bipolar geometry. The large near-IR excess of this object is similar to that of some of the A and F post-AGB stars with dusty disks and invisible binary companions (van Winckel et al. 1995). Radial velocity monitoring, near-IR spectroscopy and photometric monitoring may enable us to probe further the evolutionary status of this star.

#14: the object shows strong H_α in emission while H_β is weak, apparently filled in by emission. A weak MgII absorption line at 4481 Å and diffuse interstellar bands (DIBs) at 5783 Å and 6288 Å are visible. The colours $(I–J)_0$ and $(J–K)_0$ are consistent (Fig. 3b) with the spectral type. The moderate mid-IR excess could indicate a Vega-type star or a Herbig Be star. A second star is present $\sim 5''$ away in DENIS and 2MASS with $H = 11.5$ and $K_S = 10.2$. However, its association with the ISOGAL source appears less probable because of its substantial projected distance. The possible extension of the 7 and 15 μm source could, nevertheless, indicate a superposition of two objects.

#15: this spectrum shows a weak MgII line at 4481 Å and diffuse interstellar bands (DIBs) at 5783 Å and 6288 Å. There is a significant excess at 15 μm which could indicate a Vega-type star. However, the position of the 15 μm source at the edge of an extended emission region compromises the quality of its photometry.

#16: the spectrum (B7) is similar to #15, with DIBs at 5783 Å and 6288 Å. The H_α line is broad and partially filled in. The bump between 5000–6500 Å and the extended 15 μm emission might indicate an object with extended red emission (see text).

#17: in DENIS there is a second source with $I = 13.9$, $J = 12.8$ and $K_S = 11.3$ at a large projected distance of $11''$. However its near-IR magnitudes do not favour its association with the 7–15 μm source. The $(I-J)_0$ and $(J-K)_0$ colours of the main source are consistent. Therefore, we favour a K-giant with a mid-IR excess.

#18: in DENIS there is a second source at a large projected distance of $\sim 10''$ with $I = 11.65$, $J = 10.05$ and $K_S = 9.27$. As for source #17, we favour a K-giant with mid-IR excess.

#22: this object corresponds to a multiple system in DENIS/2MASS with projected distance of $\sim 2''$. We have not isolated the primary candidate because we suspect that the association of the visible/near-IR source and the ISOGAL source could be spurious. However, the $(I-J)_0$ and $(J-K)_0$ colours follow the temperature sequence so we favour a G-star with mid-IR excess.

#26: below 5000 Å the spectrum has poor S/N. HeI absorption lines at 5876 Å and 6678 Å may be present. It seems to be a heavily reddened early-type star. The 7 μm image shows a nearly stellar object with a jet-like structure, while at 15 μm it shows extended emission. While there is practically no excess at 7 μm, the excess at 15 μm is strong. This star is associated with IRAS 17485–2627 with high 60 μm and 100 μm fluxes ([12] < 3.19, [25] $= 13.03$, [60] $= 51.97$, [100] $= 213.30$), in a star-forming region (Codella et al. 1995). Although in J, H and K a second object has been extracted ($J = 15.7$, $H = 13.4$ and $K_S = 12.0$) at $\sim 5''$, it does not seem to be associated with the ISOGAL source. Consequently, we favour a young stellar object, with a relatively distant remnant accretion disk or cocoon, that produces the far-infrared excess.

#27: the spectrum (B3-4) is similar to that of #14, with H_α in emission and DIBs at 5783 Å and 6288 Å. There is no doubt about the association and the mid-IR excess seems reasonably well-established. The bump between 5000–6000 Å could be associated with extended red emission (see Sect. 5.3).

#28: the spectrum shows a strong reddening ($E(B-V) \sim 2.5$) with many emission lines: [OI] line at 5580 Å, H_α (H_β is not present due to reddening), P Cygni profile at 6286 Å with an emission peak at 6300 Å, [OI] emission line at 6360 Å. There is a weak emission line on the violet edge of the atmospheric feature at 6800 Å. The object seems to be a reddened early-type emission-line star. DIBs are present at 5783 Å and 6288 Å. There is no doubt about the association of optical and IR objects. The mid-IR excess is strong. However, there is some inconsistency between the 7 and 15 μm magnitudes as the [7]–[15] colour is -0.3. The object lies in a region of extended emission at 7 and 15 μm and is within 3 arcmin of the open cluster, NGC 6531.

5. Results and discussion

5.1. Cross-identification between optical spectra and ISOGAL sources

As mentioned in Sect. 4.3, we investigated the reliability of the cross-identifications between the objects for which we tool optical spectra and the actual ISOGAL sources, in order to eliminate spurious associations. Therefore, for each individual source, we examined by eye the DENIS/2MASS images in the four filters (I, J, H and K_S) as well as our ISOCAM images at 7 and 15 μm. In particular, we checked if there were second, or multiple, sources close by which might be more plausible cross-identifications than our primary target stars.

For about 50% of the sources, we did indeed find other nearby star images. Generally, these second components appear only in the J, H or K bands, and are invisible in I. We reject all such sources from further discussion although we list them in Appendix A (see the last column of Table 1). Information about the cross-identifications is given in the decription of the individual objects (Sect. 4.4 and Appendix A). In the discussion below we will take into account only those sources where there is no doubt as to

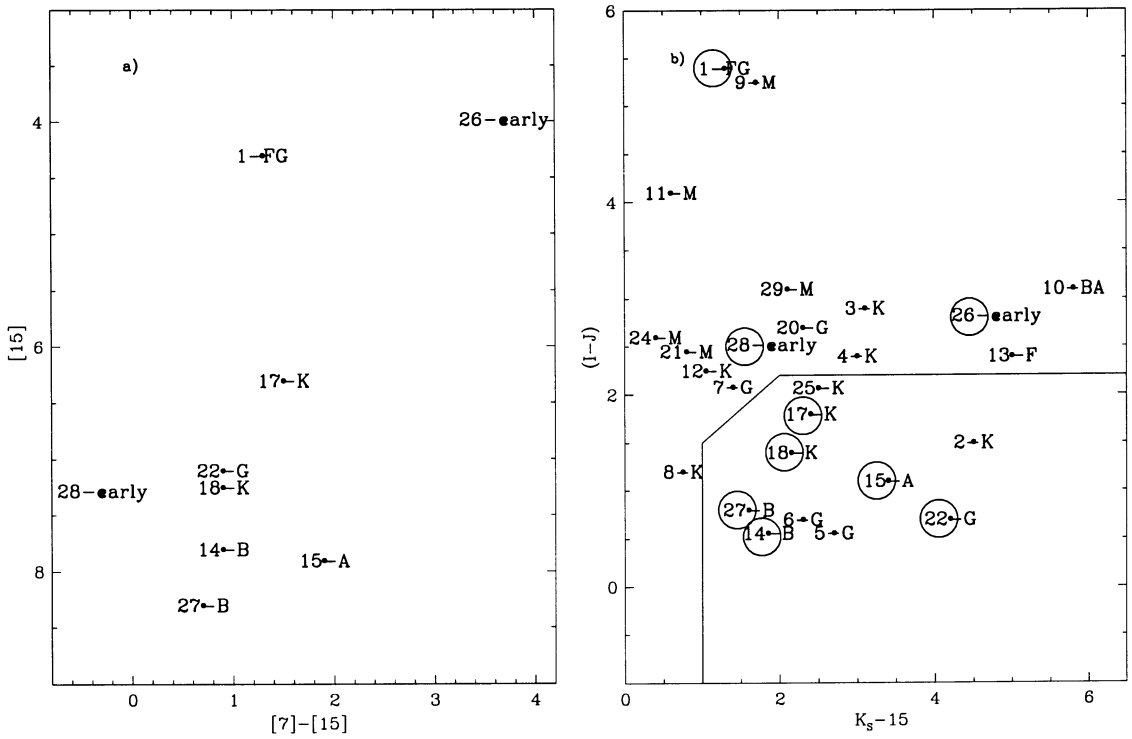

Fig. 2. [15]/[7]–[15] diagram and $(I-J)/K-[15]$ diagram of the ISOGAL spectra. Besides the spectral type, the sequence number is indicated (see Table 1). The ISOGAL sources marked with open circles are discussed in the main text, while the others are presented in the Appendix A. The lines indicate the approximate separation between early-type and late-type stars.

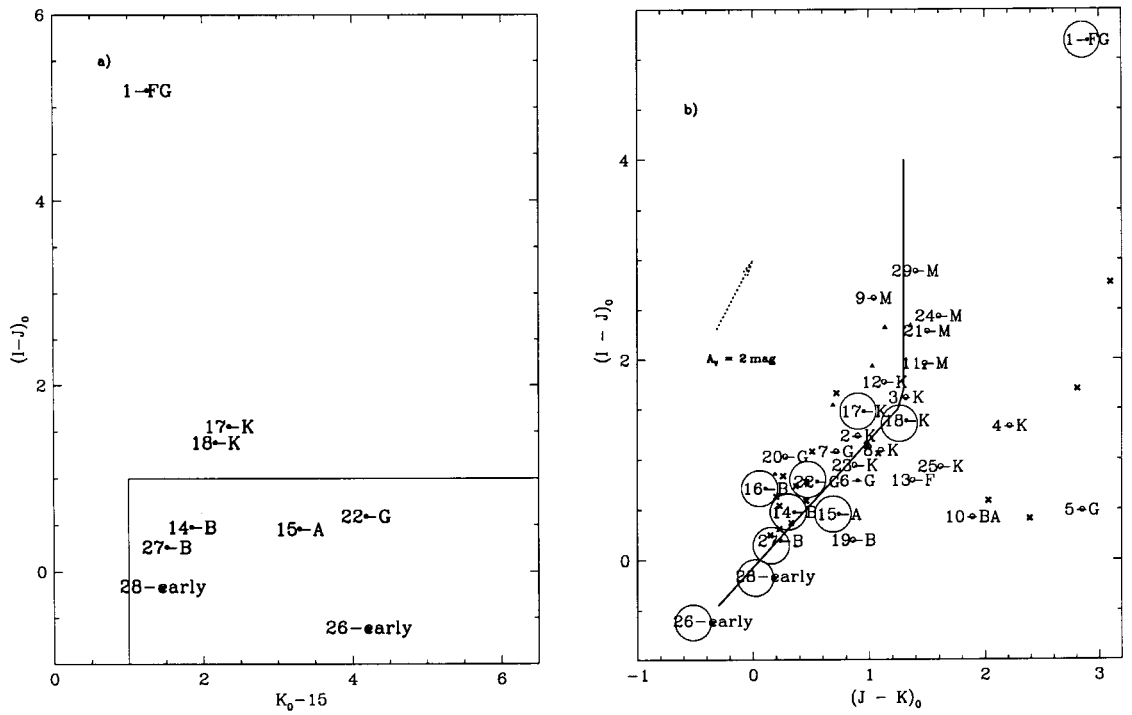

Fig. 3. $(I-J)_0/K_0-[15]$ diagram and $(I-J)_0/(J-K)_0$ diagram of the ISOGAL spectra. Besides the spectral type, the sequence number is indicated (see Table 1). The straight lines in the left panel indicate the approximate separation between early-type and late-type stars. The lines in the right panel indicate the temperature sequence for stars in the Pickles library, in the DENIS system. In Fig. 3b, a sample of hot and cold post-AGB stars is superimposed, indicated by crosses and triangles, respectively. The ISOGAL sources marked with open circles are discussed in the main text, while the others are presented in the Appendix A (see also Table 1). The extinction vector ($A_V = 2$ mag) is shown by the dotted line.

the association of the optical spectrum with the ISOGAL counterpart.

5.2. Colour-magnitude and colour-colour diagrams

The infrared colour-magnitude and colour-colour diagrams are complementary to visible spectroscopy for analysing the nature of the sources. Four of the most interesting diagrams are displayed in Figs. 2 and 3. Dereddened diagrams were produced with the estimated values of $E(B-V)$ (see Table 1), except for the [15]/[7]–[15] diagram, which is somewhat insensitive to reddening.

The [15]/[7]–[15] diagram shows that a few of the sources of Table 1 are among the brightest ISOGAL sources with a 15 μm flux up to 4 Jy, but that most of the other sources of this table are weak 15 μm ISOGAL sources. In order to ensure a reasonable level of reliability, completeness and photometric accuracy, the ISOGAL data are limited to sources brighter than 8.5 mag (8 mJy) at 15 μm and 9.75 mag (11 mJy) at 7 μm. We refer the reader to Omont et al. (1999) and Omont et al. (2002) for a detailed description of the ISOGAL catalog and its detection limits. However, the main interest of this diagram is to confirm that the sources discussed in Sect. 4.4 (sources indicated by "M" in Table 1 except #16 and #28), have a significant excess at 15 μm with respect to 7 μm. The 15 μm excess is exceptionally large in #26, and is confirmed in the $(I-J)_0/(K_0$–15) diagram. The latter suggests that $(I-J)_0$ is an efficient discrimator between early spectral types and K/M types, except in the case of the peculiar F8-G0 giant #1.

From the location in the $(I-J)_0/(K_0-[15])$ diagram of the early-type stars with infrared excess, one can determine selection criteria to seek the best candidates from the original DENIS-ISOGAL diagram, $(I-J)/(K-[15])$. This colour-colour plane is a natural one to look for non-AGB stars with circumstellar dust because of the SED difference between AGB stars and hotter objects with a circumstellar shell. Such objects are found in the domain shown in Fig. 2b. It has been designed with the dual objectives of not missing nearby early-type stars with a real mid-IR excess while limiting serious contamination by distant AGB stars.

For near-infared colours, Fig. 3b displays the $(I-J)_0/(J-K)_0$ diagram. The majority of the sources follow a sequence which is well delineated by the stellar library (temperature range between 2500 K to 35 000 K) of Pickles (1998); such DENIS colours were calculated using the DENIS filter profiles and the mean atmospheric transmission at La Silla. The few objects on the right of this sequence could be either cold pre-planetary nebulae with K excess (as defined by displaying known examples in Fig. 3b), or the result of a spurious association of a red JK source with a faint blue I star. Coupled with visual inspection of the DENIS images, this diagram indicates whether the photometry is affected by a nearby source.

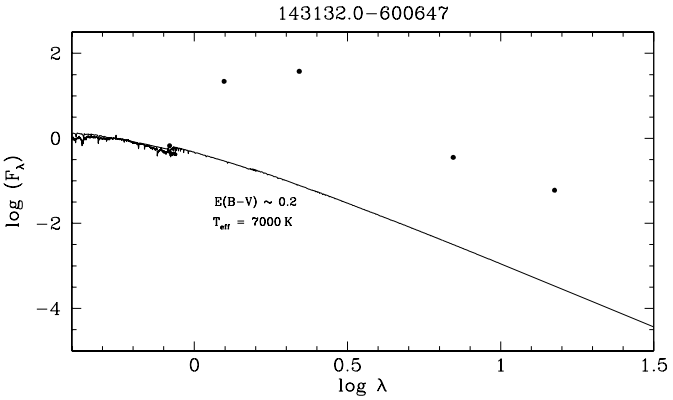

Fig. 4. Spectral energy distribution of object #1 (F8-G0III). A Kurucz model with $T_{\rm eff} = 7000$ K and a $E(B-V) \sim 0.2$ gives the best agreement to the spectrum. Note the strong near and mid-IR excess of this object.

5.3. A and B spectral types

Although our sample suffers from small number statistics, the proportions of stars with various spectral types from B to K seem to be rather comparable to those of local Hipparcos stars with 25 μm IRAS excesses (Knauer et al. 2001). The majority of the stars retained have a mid-infrared excess associated with A or B spectral type. They probably belong to one of the important classes well studied by IRAS:

- Young stars of intermediate mass with circumstellar dust. The most prominent are Herbig Ae-Be stars (nebulous emission-line stars: see e.g. Waters & Waelkens 1998). However, other young A-B stars with similar infrared properties are also known without emission lines (see e.g. the analysis of IRAS sources in the molecular cloud L1641 by Strom et al. 1989);
- $B_{[e]}$ with circumstellar emission lines (e.g. Hummel et al. 2001);
- Vega or β Pic-like circumstellar debris disks. Although such disks are better detected at longer wavelength, the sensitivity of ISOGAL is such that stars similar to β Pic should be detectable out to ∼1 kpc;
- Post-AGB stars with infrared excess should be readily detected throughout the whole Galaxy. However, they are rare and mostly distant, so that our selection criteria will miss them in regions of high extinction.

Emission lines are found in 4 objects (Hα emission is spectacular in #10, but the association of the spectrum with the mid-infrared excess is dubious). The most probable explanation of such spectra would be Herbig Ae-Be stars.

It is also likely that #26 is a young star, since it is located in the direction of a star-forming region with high extinction. The case of #15 is not clear and it remains an interesting candidate for a β Pic-type object at ∼1 kpc. High-resolution spectra are essential to pursue the exact nature of such stars.

5.4. A-B stars with a red excess

Two of the B stars are found to show a bump between 5000 and 6000 Å which could be due to extended red emission (ERE). The most well-known object with ERE is the post-AGB star with the reflection nebula known as "The Red Rectangle" (HD 44179) (Schmidt et al. 1980). The red excess is clearly seen in the spectra of #27 and #16, and perhaps in #14. ERE occurs in a wide variety of objects (Witt & Boroson 1990; Gordon et al. 1998), including reflection nebulae such as NGC 2023 and NGC 7023, while Darbon et al. (2000) found evidence of ERE in compact HII regions.

The ERE in the spectrum of the Red Rectangle appears to be due to several unidentified systems of emission bands (Schmidt et al. 2001), although CH^+ has been identified in the blue (Balm & Jura 1993). The ERE models of Seahra & Duley (1999) predict a spectrum with three peaks at 0.5, 0.7 and 1 μm which are due to carbonaceous components of interstellar matter, while Gordon et al. (2000) explain the ERE band by silicon nanoparticles. Witt et al. (1998) found that silicon nanoparticles provide the best match to the spectrum and to the photoluminescence efficiency required by the ERE.

The presence of ERE in some of our B and A-type objects with H_α emission suggests that they may be also illuminate reflection nebulae. High-resolution imaging in the H_α line and high-resolution spectroscopy may enable us to further understand the evolutionary stage, chemical composition, and ERE of these stars.

Two objects with ERE in our limited sample may be significant. However, to estimate the frequency of occurrence of ERE among dusty A and B-stars requires a systematic spectral survey of a large number of ISOGAL-DENIS sources, which is beyond the scope of the present paper.

5.5. FGK spectral types

We also found that a few of our ISOGAL sources show the type of mid-IR excess associated with F, G and K-giants. Some of these could be post-asymptotic giant branch stars (Oudmaijer et al. 1992; Pottasch & Parthasarathy 1988), as suggested for FG-type Hipparcos stars (Knauer et al. 2001). In addition to five cases with dubious associations, we have two good candidates for such objects: #22 and the remarkable case of the F8-G0 giant #1 (see Sect. 4.4).

Zuckerman et al. (1995) and Plets et al. (1997) found from an analysis of the IRAS point source catalogue that about one percent of G and K-giants have warm circumstellar dust. The presence of substantial dust near these stars is not easily explained and various mechanisms have been proposed: binarity; evaporation of circumstellar debris; or mass-loss on the first-ascent giant branch which could be related to the overabundance of lithium observed in a fraction of these late-type giants (de la Reza et al. 1996, 1997; Jasniewicz et al. 1999; Fekel & Watson 1998). First-ascent giants are not expected to have significant mass-loss and circumstellar dust shells. It is, therefore, vital to study these objects with high spectral resolution in order to understand their chemical composition and the origins of their circumstellar shells.

6. Conclusions

We have obtained low-resolution spectra and IR data of 29 ISOGAL sources. After careful inspection of the DENIS/2MASS images and of the cross-identification between ISOGAL and DENIS, about 50% of the objects have been rejected due to the influence of nearby components. Six of the stars retained have A or B spectral type, probably mostly young stars. Two of these show an extended red emission (ERE) indicating that they may be similar to the Red Rectangle or to reflection nebulae. The spectral energy distribution of object #1 suggests that it is probably a post-AGB stage in a binary system where the dust is trapped in a disc.

The $(I-J)_0/(K_0-[15])$ and $(J-K)/(K-[15])$ diagrams provide the most suitable tools to distinguish between early-type and late-type spectral types. The region of the $(I-J)/K-[15]$ diagram delineated in Fig. 2b is appropriate for a systematic search for nearby early-type objects with infrared excess.

Acknowledgements. We would like to thank M. Gerbaldi and I. S. Glass for reading the manuscript and for the fruitful discussions.

MP thanks the IAP for their hospitality during visits financed by the Indo-French IFCPAR collaboration project 1910-1.

MS is supported by the Fonds zur Förderung der wissenschaftlichen Forschung (FWF), Austria, under the project number J1971-PHY.

MC thanks NASA for its supporting this work through the ISO block grant to UC-Berkeley under contract 961501 through JPL.

The DENIS project is supported in France by the Institut National des Sciences de l'Univers, the Education Ministry and the Centre National de la Recherche Scientifique, in Germany by the State of Baden-Würtemberg, in Spain by the DGICYT, in Italy by the Consiglio Nazionale delle Ricerche, in Austria by the Fonds zur Förderung der wissenschaftlichen Forschung und Bundesministerium für Wissenschaft und Forschung.

This publication makes use of data products from the Two Micron All Sky Survey, which is a joint project of the University of Massachusetts and the Infrared Processing and Analysis Center/California Institute of Technology, funded by the National Aeronautics and Space Administration and the National Science Foundation.

Appendix A: Rejected sources

#2: this source is a very bright ISOGAL source. In K_S there is a second component 4″ away with $K_S \sim 9.0$, but this object is invisible in I and J. This second object is more likely to be associated with the ISOGAL source, while the IJK DENIS source corresponds to the observed visible spectrum.

#3: this object shows a strong feature at 6230 Å where TiO and perhaps CaOH are present. There is a second DENIS source ($J = 14.8$ and $K_S = 12.1$), $\sim 1''$ away, so that the association of the ISOGAL source with the observed visible spectrum is uncertain.
#4: the S/N of this spectrum is low but the FeI 5250 Å feature is strong. At 7 and 15 μm the object is embedded in extended emission. The quality of DENIS images in J and K is poor but, in DENIS I, there is no sign of a double component. However, the $(J-K)$ and $(I-J)$ colours do not correspond to the temperature sequence, so that the association of the I source, its observed visible spectrum (K4), and the J–K–ISOGAL source is uncertain.
#5: the spectrum (G4) is very similar to that of #1, with a strong IR excess. A double source in DENIS (projected distances of $3.2''$ (primary candidate) and $\sim 2''$), and inconsistent $(I-J)/(J-K)$ colours make the association between the I source, its observed visible spectrum, and the ISOGAL source very questionable.
#6: the spectrum (G4) is similar to that of #1. At 7 μm the source has been rejected from the new ISOGAL catalog. The ISOGAL association flag makes the cross-identification between the DENIS and the weak 15 μm ISOGAL source questionable.
#7: the S/N of this spectrum is very weak below 5000 Å, due to strong reddening ($E(B-V) \sim 1.0$). A second component in DENIS (projected distance of $2''$) with $J \sim 12.6$, $K_S \sim 12.6$ and no detection in I makes any association with our ISOGAL source dubious.
#8: this weak ISOGAL object shows a double source in DENIS. The second component (projected distance of $\sim 2''$) is not extracted by DENIS or 2MASS.
#9: below 6500 Å the spectrum has no detectable flux, suggesting strong reddening ($E(B-V) \sim 2.6$). The object has a strong near- and mid-IR excesses and is an AGB star with high mass-loss.
#10: the spectrum shows very strong H_α emission and emission lines at 4580 Å and 5070 Å. The stellar continuum is weak below 5200 Å; H_β is not visible perhaps due to the heavy reddening ($E(B-V) \sim 2.5$). There is a significant near-IR, and a large mid-IR, excess. It could be an Ae-Be Herbi-type star. However, in the DENIS I image, a second very faint component ($\sim 2''$ away) is seen but was not extracted by DENIS.
#11: this is a heavily reddened M giant ($E(B-V) \sim 2.0$) with little near- or mid-IR excess. A double component (projected distance of $\sim 3''$) appears with $J \sim 13.5$, $H \sim 11.9$ and $K_S \sim 11.5$.
#12: the spectrum (K5) is similar to #3. The TiO band at 6230 Å is relatively strong. A second component at $\sim 5''$) is visible in DENIS (not extracted by DENIS/2MASS). The mid-IR excess is relatively weak and needs confirmation.
#13: the late-F visible spectrum is similar to #7. However, there is a strong mid-IR excess and a significant near-IR excess. Such colours are known for some post-AGB stars. However, a companion is visible in the DENIS image (projected distance of $\sim 2''$), which has been not extracted by DENIS and 2MASS. The inconsistent $(J-K)_0$ and $(I-J)_0$ colours may, therefore, be due to a line-of-sight coincidence between an F-star and an AGB star.
#19: the absorption spectrum shows a weak MgII line at 4481 Å and DIBs at 5783 Å and 6288 Å. The strong near-IR and mid-IR excesses might indicate a Vega-type star, or even a post-AGB star. However, in DENIS a second red source is located $\sim 3''$ away with $K_S = 11.6$ and no I or J detection. The anomalous $(I-J)_0$ and $(J-K)_0$ colours could be contaminated by the second component. In addition, there is no confirmed 15 μm detection, and the photometry at 7 μm could be affected by extended emission present in this region.
#20: this object is a multiple system in DENIS/2MASS (projected distance of $\sim 2''$) whose other components are not extracted by DENIS/2MASS. The $(I-J)$ and $(J-K)$ colours indicate that the photometry might be affected by a second component. At 7 and 15 μm, the region is very crowded.
#21: the spectrum shows an M star with a stellar continuum below 5000 Å.
#23: the continuum below 5000 Å is weak due to strong reddening ($E(B-V) \sim 1.5$). The very faint point source at 7 μm and the lack of confirmation of a 15 μm counterpart in the present ISOGAL catalog do not confirm the presence of a mid-IR excess.
#24 this object is an M-giant with almost no detectable IR excess.
#25: this is a double source in DENIS/2MASS (projected distance of $\sim 2''$) which has not been extracted. The $(I-J)$ and $(J-K)$ colours suggest a spurious identification between the ISOGAL and the DENIS sources.
#29: this is a late M-giant with strong near- and mid-IR excesses. It is associated with a known Mira Variable star (V1547 Sgr), with a period of ∼360 days.

References

Balm, S. P., & Jura, M. 1993, ASP Conf. Ser., 45, 137
Cesarsky, C., Abergel, A., Agnese, P., et al. 1996, A&A, 315, L32
Codella, C., Palumbo, G. G. C., Pareschi, G., et al. 1995, MNRAS, 276, 57
Darbon, S., Zavagno, A., Perrin, J.-M., et al. 2000, A&A, 364, 723
Fekel, F. C., & Watson, L. C. 1998, AJ, 116, 2466
Glass, I. S., Ganesh, S., Alard, C., et al. 1999, MNRAS, 308, 127
Gordon, K. D., Witt, A. N., Rudy, J., et al. 2000, ApJ, 544, 859
Gordon, K. D., Witt, A. N., & Friedmann, B. C. 1998, ApJ, 498, 522
Hummel, W., Gässler, W., Muschielok, B., et al. 2001, A&A, 371, 932
Jacoby, G. H, Hunter, D. A., & Christian, C. A. 1984, ApJS, 56, 257
Jasniewicz, G., Parthasarathy, M., de Laverny, P., et al. 1999, A&A, 342, 831

Kerr, T. H., Hurst, M. E., Miles, J. R., & Sarre, P. J. 1999, MNRAS, 303, 446
Knauer, T. G., Ivezic, Z., & Knapp, G. R. 2001, ApJ, 552, 787
Massey, P., & Strobel, K. 1988, ApJ, 328, 315
Ojha, D. K., Sivarani, T., Parthasarathy, M., et al. 2000, Bull. Astron. Soc. India, 28, 697
Omont, A., Ganesh, S., Alard, C., et al. 1999, A&A, 348, 755
Omont, et al. 2002, A&A, in preparation
Oudmaijer, R. D., van der Veen, W. E. C. J., & Waters, L. B. F. M. 1992, A&AS, 96, 625
Parthasarathy, M., Pottasch, S. R., & Wamsteker, W. 1988, A&A, 203, 117
Parthasarathy, M., Garvía-Lario, P., Gauba, G., et al. 2001, A&A, 376, 941
Pérault, M., Omont, A., Simon, G., et al. 1996, A&A, 315, L165
Plets, H., Waelkens, C., Oudmaijer, R., et al. 1997, A&A, 323, 513
Pottasch, S. R., & Parthasarathy, M. 1988, A&A, 192, 182
Pickles, A. J. 1998, PASP, 110, 863
de la Reza, R., Drake, N. A., & da Silva, L. 1996, ApJ, 456, L115
de la Reza, R., Drake, N. A., da Silva, L., et al. 1997, ApJ, 482, L77
Seahra, S. S., & Duley, W. W. 1999, ApJ, 520, 719
Schmidt, G. D., Cohen, M., & Margon, B. 1980, ApJ, 239, L133
Schuller, et al. 2002, A&A, in preparation
Skrutskie, M. F. 1998, in The Impact of Large Scale Near-IR Sky Surveys, ed. Epchtein (Kluwer), 11
van de Steene, G. C., van Hoof, P. A. M., & Wood, P. R. 2000, A&A, 362, 984
Stone, R. P. S. 1977, ApJ, 218, 767
Strom, K. M., Margulis, M., & Strom, S. E. 1989, ApJ, 346, L33
Torres-dodgen, A. V., & Weaver, W. B. 1993, PASP, 105, 693
Turnshek, D. E., Turnshek, D. A., Craine, E. R., & Boeshaar, P. C. 1985, An atlas of digital spectra of cool stars, (Western Research Company, Tucson, Arizona)
van Winckel, H., Waelkens, C., & Waters, L. B. F. M. 1995, A&A, 293, L25
Walborn, N. R. 1980, ApJS, 44, 535
Waters, L. B. F. M., & Waelkens, C. 1998, ARA&A, 36, 233
Witt, A. N., Gordon, K. D., & Furton, D. G. 1998, ApJ, 501, L111
Witt, A. N., & Boroson, T. A. 1990, ApJ, 355, 182
Yamashita, Y., Nariai, K., & Norimoto, Y. 1977, An atlas of representative stellar spectra (University of Tokyo Press)
Zuckerman, B., Kim, S., & Liu, T. 1995, ApJ, 446, L79

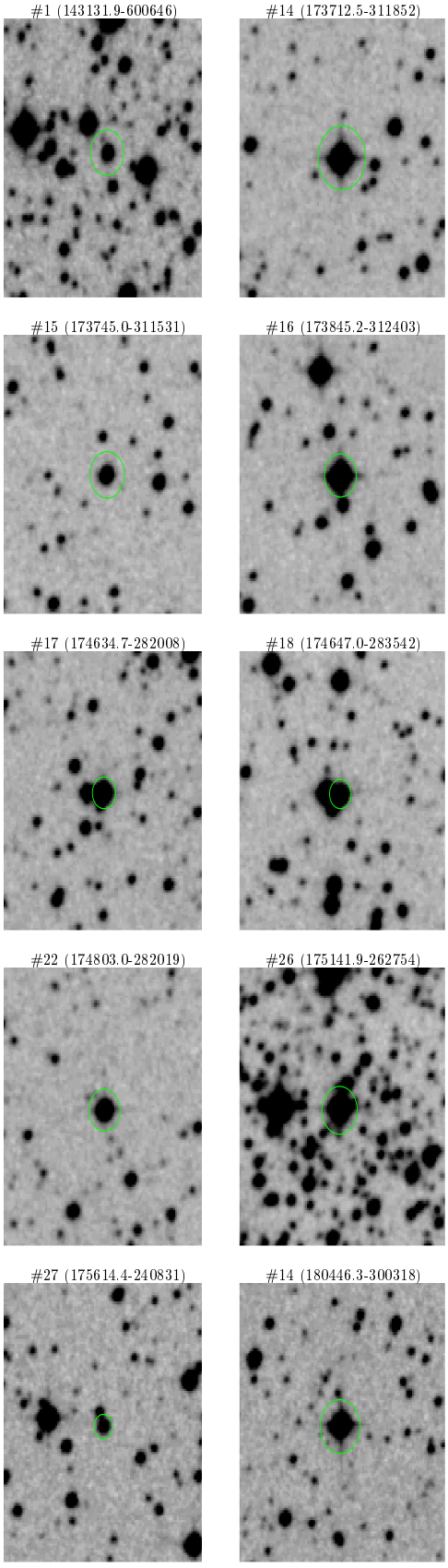

Fig. A.1. Finding charts in R of ISOGAL objects from the ESO online Digitized Sky Survey (DSS2). The field of view is $2' \times 2'$ around the center of the object. North is up and east is left. See Table 1 for the correspondence with the coordinates.